

Dynamic Modeling and Control for an Offshore Semisubmersible Floating Wind Turbine

Yingjie Gong, Qinmin Yang, *Senior Member, IEEE*, Hua Geng, *Fellow, IEEE*, Wenchao Meng, *Senior Member, IEEE*, Lin Wang

Abstract—Floating wind turbines (FWTs) hold significant potential for the exploitation of offshore renewable energy resources. Nevertheless, prior to the construction of FWTs, it is imperative to tackle several critical challenges, especially the issue of performance degradation under combined wind and wave loads. This study initiates with the development of a simplified nonlinear dynamical model for a semi-submersible FWT. In particular, both the rotor dynamics and the finite rotations of the platform are considered in presented modeling approach, thereby effectively capturing the complex interplay between the platform, tower, nacelle, and rotor under combined wind and wave loads. Subsequently, based on the developed FWT model, a novel adaptive nonlinear pitch controller is formulated with the goal of striking a trade-off between regulating power generation and reducing platform motion. Notably, the proposed control strategy adopts a continuous control approach, strategically beneficial in circumventing the chattering phenomenon commonly associated with sliding mode control. Furthermore, the controller integrates an online approximator and a robust integral of the sign of the tracking error, facilitating real-time learning of system unknown dynamics while compensating for bounded disturbances. Finally, both the accuracy of the established nonlinear FWT model in predicting key dynamics and the superiority of the presented pitch controller are validated through comprehensive comparative studies.

Note to Practitioners—This paper addresses the conflicting goals between power regulation and load mitigation for floating wind turbines (FWTs) to ensure the reliable operation of wind turbine systems. This remains an ongoing challenge due to the inherent complexity of existing FWT models, frequently resulting in controllers crafted using linearized representations that fail to accommodate real-world uncertainties effectively. Through the utilization of a simplified physical-based nonlinear FWT model, a novel adaptive nonlinear pitch controller emerges as a promising solution. Notably, the developed nonlinear FWT model elucidates the coupling between rotor and platform degrees of freedom clearly and succinctly, facilitating the design of intelligent controllers. Our approach demonstrates the capability to concurrently regulate power production and stabilize the platform. Additionally, an online approximator is integrated into the controller to capture system dynamics, thus augmenting adaptability and diminishing reliance on high-gain feedback compensation. Importantly, this control strategy holds promise for extension and implementation in various other renewable energy systems.

Index Terms—Floating wind turbines, adaptive pitch control, robustness, load mitigation.

I. INTRODUCTION

GIVEN the predominant concentration of wind energy in deep-sea areas, the last few decades have witnessed a swift rise in the advancement of floating wind turbines (FWTs) [1], [2], [3]. Unlike bottom-fixed WTs, FWTs experience a more intricate dynamic behavior due to the combined influence of wind and wave loads. Moreover, the dynamic performance of FWTs may undergo notable degradation due to the motion of the floating platform, even when mooring lines anchor the FWT to the seabed [4]. Therefore, devising adaptive and robust control strategies that improve power output while minimizing platform motion remains a primary challenge in FWTs.

Initially, the characteristic analysis of FWTs under wind and wave loads is pivotal in devising a well-designed controller, which highlights that an effective mathematical model is the foundation for illustrating the nonlinear dynamics of FWTs in controller design. Various studies have explored modeling approaches for different types of FWTs, such as the high-fidelity fatigue, aerodynamics, structures, and turbulence (FAST) model proposed by the National Renewable Energy Laboratory (NREL) [5]. This model excels in detailing FWTs' dynamics, but its complexity renders it impractical for controller design applications. By contrast, simplified models, striking a judicious balance between conciseness and accuracy, have emerged as a more pragmatic option. In [6], [7], the 2-degree-of-freedom (2-DOF) reduced-order models were introduced for barge, TLP, and spar types of FWTs, while a 3-DOF dynamic model was developed in [8] specifically for a barge-type FWT. Then to address out-of-plane motions and reduce fatigue damage, a control-oriented rigid offshore WT was introduced in [9] based on the first principles, and subsequent consideration of structural flexibility was presented in [10].

Nonetheless, it is important to note that the prevalent modeling approaches predominantly presume a static or constant rotor rotational speed, overlooking the fact that dynamic variations in rotor speed significantly affect the aerodynamic loads and the rotor's gyroscopic moment, thereby altering the system's overall responses. Consequently, to improve the accuracy of the FWT system's dynamic behaviors, integrating rotor dynamics into the system's overall dynamics is essential [11]. Furthermore, despite expectations of increased focus on semi-submersible FWTs (SSFWTs) in future developments

Y. Gong and W. Meng are with the State Key Laboratory of Industrial Control Technology, College of Control Science and Engineering, Zhejiang University, Hangzhou 310027, China.

Q. Yang is with the State Key Laboratory of Industrial Control Technology, College of Control Science and Engineering, and the Huzhou Institute, Zhejiang University, Hangzhou 310027, China.

H. Geng is with the Department of Automation, Beijing National Research Center for Information Science and Technology, Tsinghua University, Beijing 100084, China.

L. Wang is with the Zhejiang Windey Co. Ltd., Hangzhou 310027, China.

[1], research on the coupled dynamic models of SSFWTs remains limited, especially when compared to other FWT designs, particularly the spar-type FWTs. Consequently, there is a critical need to develop a comprehensive dynamic model for SSFWTs that incorporates rotor dynamics. This model will facilitate more effective control design strategies, ultimately improving controller performance.

In addition, the main control goal for FWTs in region III is to regulate power production at its rated value by adjusting blade pitch angles [12]. However, the direct application of traditional controller originally designed for “standard onshore” WT tends to be inefficient for FWTs, which is primarily attributed to the additive motions of floating platforms [13], [14]. Thus, it is important for FWTs to enhance the system damping and stabilize overall performance. In [15], extensive analyses of blade pitch control had been conducted on three main platforms, which effectively mitigated power fluctuations and platform motion. Meanwhile, some advanced control algorithms, such as linear quadratic regulator-based controllers [16], [17] and model predictive control [18] have been examined to address the damping of FWTs. Although these methods can achieve better power regulation and structural load mitigation than the baseline controller [19], an obvious limitation of these methods is the reliance on the conventional linear models as a prevalent routine, and thus exhibit performance degradation outside the linearization points [20], [21].

An effective solution to address these limitations is to use nonlinear control theory. Notably, a nonlinear controller known as sliding mode control (SMC) has recently been implemented in the context of vibration mitigation for a barge-type FWT in [22]. It is crucial to highlight that SMC stands out as one of the most potent nonlinear control techniques documented in the literature, adept at addressing uncertainties and disturbances stemming from wind-wave joint excitation. However, despite its commendable robustness, SMC is plagued by the well-documented chattering phenomenon resulting from its discontinuous behavior. Furthermore, the sliding mode controller typically employs conservative control gains to ensure effective performance in the presence of disturbances. To augment control performance, a second-order SMC based control algorithm, reducing the chattering, has been applied in [23], [24], [25] to achieve power regulation for spar-type FWTs. Unfortunately, a significant drawback lies in the reliance on applied the linear model framework in this approach, treating the FWT system as a black box for direct execution of SMC. This oversight neglects detailed wind/wave descriptions and known system parts, resulting in excessive SMC effects that amplify damage to the pitch actuator.

Motivated by the aforementioned issues, the primary objective of this paper is to formulate a simplified nonlinear model for SSFWTs. Subsequently, leveraging the established model, we design a robust adaptive pitch controller employing a continuous control scheme. The contributions of this paper can be summarized as:

- 1) An improved modeling approach for SSFWT is proposed considering rotor dynamics and finite platform rotations. The resulting model is succinctly presented in matrix form with clearly defined elements, facilitating

more effective control strategies design and ultimately enhancing controller performance.

- 2) Based on the established model, a new robust nonlinear pitch controller has been developed to achieve a trade-off between the rotor speed regulation and suppressing the platform motion of SSFWT.
- 3) In comparison to exist nonlinear controllers, such as SMC, an online approximator is utilized to learn the unknown system dynamics, thereby enhancing the controller’s adaptability and reducing the reliance on high-gain feedback compensation.

This paper is structured as follows: Section II introduces the modeling of SSFWT. In Section III, we present a novel blade pitch controller and then demonstrate its stability. Section IV shows verification results conducted on a SSFWT, followed by the conclusion of this study is given in Section V.

II. MODELING OF THE SSFWT SYSTEM

The schematic diagram of the SSFWT is depicted in Fig. 1. Meanwhile, the dynamic characteristics of SSFWT are intricately influenced by four principal mechanical components:

- 1) **Floating Platform:** Characterized by mass m_p , center of mass G_p and inertia tensor $\mathbf{I}_p = \text{diag}\{I_{p_x}, I_{p_y}, I_{p_z}\}$.
- 2) **Tower:** Comprising mass m_t , center of mass G_t and inertia tensor $\mathbf{I}_t = \text{diag}\{I_{t_x}, I_{t_y}, I_{t_z}\}$. The tower supports the rotor-nacelle assembly, and the yaw motion is not considered.
- 3) **Nacelle:** Featuring mass m_{n_c} , center of mass G_{n_c} and inertia tensor $\mathbf{I}_n = \text{diag}\{I_{n_x}, I_{n_y}, I_{n_z}\}$.
- 4) **Rotor:** Represented as a rigid disc with angular velocity $\Omega_r(t)$, mass m_r , center of mass G_r and inertia tensor $\mathbf{I}_r = \text{diag}\{I_{r_x}, I_{r_y}, I_{r_z}\}$.

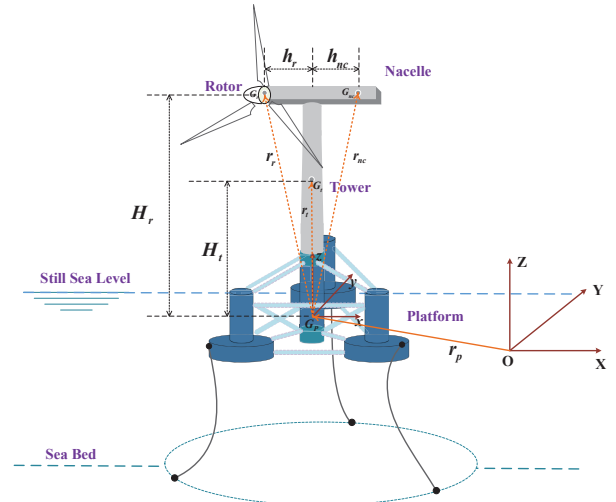


Fig. 1: Schematic diagram of the SSFWT.

Note that two right-handed Cartesian coordinate frames, \mathcal{F}_I (inertial frame) and \mathcal{F}_p (body-fixed frame), are defined in Fig. 1. The origin of \mathcal{F}_I is located at the platform’s center of gravity (G_p) before any displacement, with its unit vector

$[\hat{\mathbf{e}}_3]_I$ oriented vertically upward. The unit vectors $[\hat{\mathbf{e}}_1]_I$ and $[\hat{\mathbf{e}}_2]_I$ are horizontally aligned, parallel to the Earth's surface. Conversely, \mathcal{F}_p is affixed to G_p and initially coincides with \mathcal{F}_I in the absence of wind or wave disturbances. It's noteworthy that the subscript denotes the vector representation frame in this analysis, whereas vectors lacking superscripts denote representation in any arbitrary frame. Furthermore, the principal axes associated with the inertia tensor of rigid components align with \mathcal{F}_p .

A. System kinematics

The floating platform typically exhibits six DOFs in frame \mathcal{F}_I : three for translation (surge, sway, and heave) and three for rotation (roll, pitch, and yaw), denoted by

$$\mathbf{r}_p = [r_x \ r_y \ r_z]^T, \quad \boldsymbol{\theta}_p = [\theta_x \ \theta_y \ \theta_z]^T$$

where \mathbf{r}_p represents translational displacements of the origin of frame \mathcal{F}_p with respect to frame \mathcal{F}_I , expressed in \mathcal{F}_I . Meanwhile, the rotational angles are characterized by the Euler angle triad $\boldsymbol{\theta}_p$. The 3-2-1 Euler angle sequence [26] characterizes finite rotation in this paper. The rotation matrix \mathbf{R} in (1) facilitates the transformation of vectors between frames \mathcal{F}_p and \mathcal{F}_I .

$$\mathbf{R} = \begin{bmatrix} c_{\theta_z} c_{\theta_y} & c_{\theta_z} s_{\theta_y} s_{\theta_x} - s_{\theta_z} c_{\theta_x} & c_{\theta_z} s_{\theta_y} c_{\theta_x} + s_{\theta_z} s_{\theta_x} \\ s_{\theta_z} c_{\theta_y} & s_{\theta_z} s_{\theta_y} s_{\theta_x} + c_{\theta_z} c_{\theta_x} & s_{\theta_z} s_{\theta_y} c_{\theta_x} - c_{\theta_z} s_{\theta_x} \\ -s_{\theta_y} & c_{\theta_y} s_{\theta_x} & c_{\theta_y} c_{\theta_x} \end{bmatrix} \quad (1)$$

where $c_{(\cdot)} = \cos(\cdot)$ and $s_{(\cdot)} = \sin(\cdot)$. Subsequently, the translational velocity of the platform within the frame \mathcal{F}_p can be denoted as

$$[\mathbf{v}_p]_p = [v_x, v_y, v_z]^T = \mathbf{R}^T [\dot{\mathbf{r}}_p]_I \quad (2)$$

Also, the Euler kinematical equation of the 3-2-1 Euler angle sequence is

$$[\dot{\boldsymbol{\theta}}_p]_I = \mathbf{J}[\boldsymbol{\omega}_p]_p = \begin{bmatrix} 1 & \frac{s_{\theta_x} s_{\theta_y}}{c_{\theta_y}} & \frac{c_{\theta_x} s_{\theta_y}}{c_{\theta_y}} \\ 0 & c_{\theta_x} & -s_{\theta_x} \\ 0 & \frac{s_{\theta_x}}{c_{\theta_y}} & \frac{c_{\theta_x}}{c_{\theta_y}} \end{bmatrix} \begin{bmatrix} \omega_x \\ \omega_y \\ \omega_z \end{bmatrix} \quad (3)$$

where $[\boldsymbol{\omega}_p]_p = [\omega_x \ \omega_y \ \omega_z]^T$ indicates the angular velocity of the platform in the frame \mathcal{F}_p . Further, the kinetic energy (KE) and potential energy (PE) of the floating platform are

$$\begin{cases} \mathcal{T}_p = \frac{1}{2} m_p [\mathbf{v}_p^T]_p [\mathbf{v}_p]_p + \frac{1}{2} [\boldsymbol{\omega}_p^T]_p (\mathbf{I}_p [\boldsymbol{\omega}_p]_p), \\ \mathcal{V}_p = m_p g r_z \end{cases} \quad (4)$$

Furthermore, as depicted in Fig. 1, the position vectors in frame \mathcal{F}_p for the centers of mass of the tower (G_t), nacelle (G_{nc}), and rotor (G_r) are described by

$$\begin{aligned} [\mathbf{r}_{G_t}]_p &= [0 \ 0 \ H_t]^T, & [\mathbf{r}_{G_{nc}}]_p &= [h_{nc} \ 0 \ H_r]^T \\ [\mathbf{r}_{G_r}]_p &= [-h_r \ 0 \ H_r]^T \end{aligned}$$

Meanwhile, the velocities of these center of masses can be formulated by

$$\begin{aligned} \mathbf{v}_t &= \mathbf{v}_p + \boldsymbol{\omega}_p \times \mathbf{r}_{G_t}, & \mathbf{v}_{nc} &= \mathbf{v}_p + \boldsymbol{\omega}_p \times \mathbf{r}_{G_{nc}} \\ \mathbf{v}_r &= \mathbf{v}_p + \boldsymbol{\omega}_p \times \mathbf{r}_{G_r} \end{aligned}$$

Moreover, it is evident that the platform, tower, and nacelle share a common angular velocity denoted as $\boldsymbol{\omega}_p$, while the rotor's angular velocity is $\boldsymbol{\omega}_r = \boldsymbol{\omega}_p + \boldsymbol{\Omega}_r$ and the rotor spin rate is $[\boldsymbol{\Omega}_r]_p = \boldsymbol{\Omega}_r \cdot [\hat{\mathbf{e}}_1]_p$. Subsequently, the KE and PE of the tower, the nacelle, and the rotor are derived, respectively, denoted by:

$$\begin{cases} \mathcal{T}_t = \frac{1}{2} m_t [\mathbf{v}_t^T]_p [\mathbf{v}_t]_p + \frac{1}{2} [\boldsymbol{\omega}_t^T]_p (\mathbf{I}_t [\boldsymbol{\omega}_t]_p), \\ \mathcal{V}_t = m_t g ([\mathbf{r}_{t0}]_I \cdot [\hat{\mathbf{e}}_3]_I) \\ \mathcal{T}_{nc} = \frac{1}{2} m_{nc} [\mathbf{v}_{nc}^T]_p [\mathbf{v}_{nc}]_p + \frac{1}{2} [\boldsymbol{\omega}_{nc}^T]_p (\mathbf{I}_{nc} [\boldsymbol{\omega}_{nc}]_p), \\ \mathcal{V}_{nc} = m_{nc} g ([\mathbf{r}_{no}]_I \cdot [\hat{\mathbf{e}}_3]_I) \\ \mathcal{T}_r = \frac{1}{2} m_r [\mathbf{v}_r^T]_p [\mathbf{v}_r]_p + \frac{1}{2} [\boldsymbol{\omega}_r^T]_p (\mathbf{I}_r [\boldsymbol{\omega}_r]_p), \\ \mathcal{V}_r = m_r g ([\mathbf{r}_r]_I \cdot [\hat{\mathbf{e}}_3]_I) \end{cases} \quad (5)$$

with

$$\begin{aligned} [\mathbf{r}_{t0}]_I &= \mathbf{r}_p + \mathbf{R}[\mathbf{r}_{G_t}]_p, & [\mathbf{r}_{no}]_I &= \mathbf{r}_p + \mathbf{R}[\mathbf{r}_{G_{nc}}]_p, \\ [\mathbf{r}_{ro}]_I &= \mathbf{r}_p + \mathbf{R}[\mathbf{r}_{G_r}]_p \end{aligned}$$

Then the total KE and PE of the multibody system can be obtained by

$$\begin{aligned} \mathcal{T} &= \mathcal{T}_p + \mathcal{T}_t + \mathcal{T}_{nc} + \mathcal{T}_r \\ \mathcal{V} &= \mathcal{V}_p + \mathcal{V}_t + \mathcal{V}_{nc} + \mathcal{V}_r \end{aligned} \quad (6)$$

B. External forces

The total external forces and accompanying moments exerted on the SSFWT primarily originate from hydrostatic, hydrodynamic, aerodynamic, and mooring loads, derived by

$$\begin{aligned} \mathbf{F} &= \mathbf{F}_B + \mathbf{F}_D + \mathbf{F}_A + \mathbf{F}_M \\ \mathbf{T} &= \mathbf{T}_B + \mathbf{T}_D + \mathbf{T}_A + \mathbf{T}_M \end{aligned} \quad (7)$$

The subscripts B , D , A and M correspond to the external forces and moments mentioned above in the description.

In this study, we assume that the semi-submersible platform comprises seven homogenous and uniform cylinders, denoted as a main column ($i = 1$) and three upper side columns ($i = 2, 3, 4$) floating in the water, along with three base columns ($i = 5, 6, 7$) fully submerged. As per Archimedes' principle, the buoyant force exerted on the platform equals the weight of the fluid displaced by the platform, as determined by

$$[\mathbf{F}_B]_p = \mathbf{R}^{-1} ((\rho_w g V_d) [\hat{\mathbf{e}}_3]_I) \quad (8)$$

where ρ_w and g are the density of water and the gravitational constant, respectively; V_d denotes the total instantaneous submerged volume, satisfying

$$V_d = \sum_{i=1}^7 V_i, \quad V_i = L_i A_i = \frac{\pi}{4} L_i d_i^2, \quad i = 1, \dots, 7 \quad (9)$$

where A_i , d_i and L_i are the cross-sectional area, the diameter and length of the i th cylinder, respectively. In fact, the length L_i of the i th submerged members equals its actual length. For floating members, the magnitude of vector $[\mathbf{r}_{bf,i}]_I$, representing the vector from the base center b_i to the floating area center f_i (as depicted in Fig. 2), characterizes its length. Moreover, the submerged length L_i satisfies

$$\begin{aligned} [\mathbf{r}_{bf,i}]_I &= L_i \cdot \mathbf{R}[\hat{\mathbf{e}}_3]_p, \\ [\mathbf{r}_{bf,i}]_I \cdot [\hat{\mathbf{e}}_3]_I &= \eta_i + L_{i0} + h_{bi} \end{aligned} \quad (10)$$

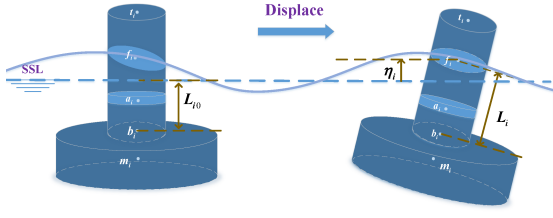


Fig. 2: Submerged length of platform floating member.

which leads to

$$L_i = \frac{\eta_i + L_{i,0} + h_{b,i}}{\mathbf{R}[\hat{\mathbf{e}}_3]_p \cdot [\hat{\mathbf{e}}_3]_I} \quad (11)$$

where the water free surface elevation, denoted as η_i , is the vertical displacement of the water surface as a wave traverses the i th floating member. $L_{i,0}$ is the initial submerged length of the cylinder; $h_{b,i}$ denotes the vertical displacement of each floating member's base center b_i , described as

$$\begin{aligned} h_{b,i} &= (\mathbf{R}(0)[\mathbf{r}_{b,i}]_p - ([\mathbf{r}_p]_I + \mathbf{R}(\theta_p)[\mathbf{r}_{b,i}]_p)) \cdot [\hat{\mathbf{e}}_3]_I \\ &= (\mathbf{R}(0) - \mathbf{R}(\theta_p))[\mathbf{r}_{b,i}]_p \cdot [\hat{\mathbf{e}}_3]_I - r_z \end{aligned} \quad (12)$$

where $[\mathbf{r}_{b,i}]_p$ represents a constant vector in \mathcal{F}_p , originating from point G_p and terminating at point b_i . Furthermore, the hydrostatic moment can be derived as

$$\mathbf{T}_{B,i}^p = [\mathbf{r}_B]_p \times [\mathbf{F}_B]_p \quad (13)$$

where $[\mathbf{r}_B]_p$ is the position vector of platform's buoyancy center in \mathcal{F}_p , which can be obtained by

$$[\mathbf{r}_B]_p = \frac{\sum_{i=1}^7 V_i \cdot [\mathbf{r}_{m_i}]_p}{V_d} \quad (14)$$

with $[\mathbf{r}_{m_i}]_p = [\mathbf{r}_{b,i}]_p + \frac{1}{2}L_i[\hat{\mathbf{e}}_3]_p$, $i = 1, \dots, 7$, being the position vector of centroid m_i in \mathcal{F}_p .

The hydrodynamic loads acting on the platform are determined utilizing the Morison equation and strip theory [27]. Initially, the hydrodynamic force acting on a submerged cylinder in transverse water flow is calculated by

$$\mathbf{F}_{dt,i} = \mathbf{F}_{1i}^t + \mathbf{F}_{2i}^t, \quad i = 1, \dots, 7 \quad (15)$$

where \mathbf{F}_{1i}^t denotes the inertial terms, \mathbf{F}_{2i}^t represent the remaining terms of Morison's equation, and they can be obtained by

$$\begin{aligned} \mathbf{F}_{1i}^t &= \int_{z_t}^{z_b} C_{D_i} \|(\mathbf{v}_{ref,i})_{\perp}\| (\mathbf{v}_{ref,i})_{\perp} + (C_{A_i} + \rho_w A_i) \\ &\quad \cdot (\dot{\mathbf{v}}_{w,i}^p)_{\perp} dz, \\ \mathbf{F}_{2i}^t &= - \int_{z_t}^{z_b} C_{A_i} (\dot{\mathbf{v}}_{a,i}^p)_{\perp} dz \end{aligned}$$

with $z_t = L_i$, $z_b = 0$, $\mathbf{v}_{ref,i} = \mathbf{v}_{w,i} - \mathbf{v}_{a,i}$, and $C_{D_i} = \frac{1}{2}C_{di}\rho_w d_i$, $C_{A_i} = C_{ai}\rho_w A_i$. Here, C_{d_i} and C_{a_i} are drag and added mass coefficients, respectively; z_t and z_b are the vertical coordinates of point f_i and point b_i in \mathcal{F}_p , respectively; The amplitude of (\cdot) is denoted by $\|(\cdot)\|$; The perpendicular component of (\cdot) with respect to the centerline of the submerged member is denoted as $(\cdot)_{\perp}$. Examining a length element dz along each submerged platform member and a specific point

a_i situated on the centerline of the i th submerged segment, positioned at a distance of z from point b_i , aligns with the centroid of the volume element, as shown in Fig. 2. Then the position vector of a_i in \mathcal{F}_p is $[\mathbf{r}_{a_i}]_p = [\mathbf{r}_{b_i}]_p + z \cdot [\hat{\mathbf{e}}_3]_p$, and the velocity and acceleration of a_i are

$$\mathbf{v}_{a,i} = \mathbf{v}_p + \omega_p \times [\mathbf{r}_{a_i}]_p, \quad \dot{\mathbf{v}}_{a,i} = \dot{\mathbf{v}}_p + \dot{\omega}_p \times [\mathbf{r}_{a_i}]_p$$

Besides, $\mathbf{v}_{w,i}$ and $\dot{\mathbf{v}}_{w,i}$ denote the corresponding velocity and acceleration of water particle coincident with points a_i in each moment. In this study, the kinematics of the wave field is established through the application of the Airy wave theory. Comprehensive calculation details can be found in [28], and for brevity, they are not expounded upon in this context.

Then from (15), the moments caused by the hydrodynamic forces can be derived by

$$\mathbf{T}_{dt,i} = \mathbf{T}_{1i}^t + \mathbf{T}_{2i}^t = \int_{z_t}^{z_b} \mathbf{r}_{a_i} \times \mathbf{F}_{dt,i}, \quad i = 1, \dots, 7 \quad (16)$$

Moreover, it is essential to highlight that the three base columns of the platform ($i = 5, 6, 7$) also experience drag and inertial forces in the heave direction. Similar to (15), these forces can be expressed as:

$$\mathbf{F}_{dh,i} = \mathbf{F}_{1i}^h + \mathbf{F}_{2i}^h, \quad i = 5, 6, 7 \quad (17)$$

where

$$\begin{aligned} \mathbf{F}_{1i}^h &= C_{D_z i} \|(\mathbf{v}_{ref,i})_{\parallel}\| (\mathbf{v}_{ref,i})_{\parallel} + C_{A_z i} (\dot{\mathbf{v}}_{w,i}^p)_{\parallel} dz, \\ &\quad + (A_i p_{b_i} - (A_i - A_{i-3}) p_{t_i}) \cdot [\hat{\mathbf{e}}_3]_p, \\ \mathbf{F}_{2i}^h &= - C_{A_z i} (\dot{\mathbf{v}}_{c_i})_{\parallel} \end{aligned}$$

with $C_{D_z i} = \frac{1}{2}C_{dz i}\rho_w A_i$, $C_{A_z i} = C_{az i}\rho_w V_{Ri}$ and $V_{Ri} = \frac{2}{3}\pi(d_i/2)^3$, where $C_{dz,i}$ and $C_{az,i}$ represent the drag and added mass coefficients along the Z -axis, respectively; p_{b_i} and p_{t_i} denote the dynamic pressure at the bottom and top faces of the heave-plate. The symbol $(\cdot)_{\parallel}$ indicates a component parallel to the centerline of the submerged member. Point c_i corresponds to the center of gravity for the i th base column, with its velocity and acceleration given by:

$$\mathbf{v}_{c_i} = \mathbf{v}_{a_i} \Big|_{z=\frac{L_i}{2}}, \quad \dot{\mathbf{v}}_{c_i} = \dot{\mathbf{v}}_{a_i} \Big|_{z=\frac{L_i}{2}}$$

Correspondingly, the moments caused by the hydrodynamic forces can be derived by

$$\mathbf{T}_{dh,i} = \mathbf{T}_{1i}^h + \mathbf{T}_{2i}^h = \mathbf{r}_{c_i} \times (\mathbf{F}_{1i}^h + \mathbf{F}_{2i}^h), \quad i = 5, 6, 7 \quad (18)$$

with $\mathbf{r}_{c_i} = \mathbf{r}_{a_i} \Big|_{z=\frac{L_i}{2}}$.

To sum up, the total hydrodynamic force and corresponding moments on the platform are

$$\begin{aligned} \mathbf{F}_D &= \sum_{i=1}^7 \mathbf{F}_{dt,i} + \sum_{j=5}^7 \mathbf{F}_{dh,j}, \\ \mathbf{T}_D &= \sum_{i=1}^7 \mathbf{T}_{dt,i} + \sum_{j=5}^7 \mathbf{T}_{dh,j} \end{aligned} \quad (19)$$

Remark 1: It is noteworthy that the inertial terms in (15)–(18), namely, \mathbf{F}_{1i}^t , \mathbf{F}_{2i}^h , \mathbf{T}_{1i}^t , \mathbf{T}_{2i}^h , are typically relocated to the left-hand side of the equation of motion. This results in the formation of an added mass matrix M_a , and its formulation

is provided in Appendix A.

Next, the primary wind-induced loads on the SSFWT involve the aerodynamic torque τ_a around the turbine shaft and the axial thrust force F_a along the shaft axis, expressed as

$$\begin{aligned} F_a &= \frac{1}{2}\rho_a\pi R_r^2 C_t(\lambda, \beta) \|(\mathbf{u}_w)\|^2 \\ \tau_a &= \frac{1}{2}\rho_a\pi R_r^3 \frac{1}{\lambda} C_p(\lambda, \beta) \|(\mathbf{u}_w)\|^2 \end{aligned} \quad (20)$$

where R_r signifies the rotor radius, while ρ_a is air density. The relative velocity between the wind and rotor is denoted by \mathbf{u}_w , which can be calculated as $\mathbf{u}_w = \mathbf{v}_w - \mathbf{v}_r$, where \mathbf{v}_w is the wind speed vector. Further, we can obtain that the component of \mathbf{u}_w and parallel to the rotor shaft axis ($[\hat{\mathbf{e}}_1]_p$) can be derived by $(\mathbf{u}_w)_\parallel = (\mathbf{u}_w \cdot [\hat{\mathbf{e}}_1]_p)[\hat{\mathbf{e}}_1]_p$. The thrust and power coefficients of WTs are denoted as C_t and C_p , respectively, which are dependent on the blade pitch angle β and the tip speed ratio λ , with $\lambda = \Omega_r R_r / \|(\mathbf{u}_w)\|$. Then the formulations of the aerodynamic force and associated moment around the origin of frame \mathcal{F}_p are as follows

$$[\mathbf{F}_A]_p = F_a[\hat{\mathbf{e}}_1]_p, \quad [\mathbf{T}_A]_p = \tau_a[\hat{\mathbf{e}}_1]_p + [\mathbf{r}_r]_p \times [\mathbf{F}_A]_p \quad (21)$$

In addition, mooring loads are evaluated utilizing the quasi-static method [29], [30]. For the detailed calculation process, readers can refer to [11], while a thorough discussion is omitted here to maintain brevity.

C. Nonlinear model of SSFWT

In order to obtain the dynamic model of SSFWT, the Lagrange's equation based on the platform's quasi-coordinates $(\mathbf{v}_p, \boldsymbol{\omega}_p)$ is utilized to derive the equations of motion (EOM) of the platform, while the EOM of the WT drivetrain is obtained from the conventional form of Lagrange's equation [31], [32]. By recalling equations (2), (3), (6), and (7), the nonlinear model of SSFWT can be derived as:

$$\bar{\mathbf{M}} \begin{bmatrix} [\dot{\mathbf{r}}_p]_I \\ [\dot{\boldsymbol{\theta}}_p]_I \\ [\dot{\mathbf{v}}_p]_p \\ [\dot{\boldsymbol{\omega}}_p]_p \\ \Omega_r \end{bmatrix} = \begin{bmatrix} \mathbf{R}[\mathbf{v}_p]_p \\ \mathbf{J}[\boldsymbol{\omega}_p]_p \\ [\mathbf{F}]_p \\ [\mathbf{T}]_p \\ \tau_a - \tau_g \end{bmatrix} + \mathbf{s}(\mathbf{r}_p, \boldsymbol{\theta}_p, \mathbf{v}_p, \boldsymbol{\omega}_p, \Omega_r) \quad (22)$$

where \mathbf{s} is a vector function about $\mathbf{r}_p, \boldsymbol{\theta}_p, \mathbf{v}_p, \boldsymbol{\omega}_p, \Omega_r$. The expressions of $\bar{\mathbf{M}}$ and \mathbf{s} are given in Appendix B.

Remark 2: Note that the simplified SSFWT model developed in (22) is primarily utilized for controller design, with subsequent validation typically conducted on the complete state model.

III. CONTROLLER DESIGN

In this section, a novel pitch controller for SSFWT is designed based on the robust integral of the sign of the error (RISE) control approach, developed in [33], and then the regulation of generator power while reducing the platform motion can be guaranteed in region III.

A. Model reformulation

Based on (22), the SSFWT model can be rewritten as

$$\dot{\mathbf{X}} = \bar{\mathbf{M}}^{-1}(\boldsymbol{\Lambda}(\mathbf{X}, \beta, \mathbf{v}_w) + \mathbf{s}(\mathbf{X})) \quad (23)$$

with $\mathbf{X} = \left[[\mathbf{r}_p^T]_I \quad [\boldsymbol{\theta}_p^T]_I \quad [\mathbf{v}_p^T]_p \quad [\boldsymbol{\omega}_p^T]_p \quad \Omega_r \right]^T$ and

$$\boldsymbol{\Lambda}^T = \left[(\mathbf{R}[\mathbf{v}_p]_p)^T \quad (\mathbf{J}[\boldsymbol{\omega}_p]_p)^T \quad [\mathbf{F}]_p^T \quad [\mathbf{T}]_p^T \quad \tau_a - \tau_g \right]$$

For the purpose of controller design, the external load vector $\boldsymbol{\Lambda}$ is divided as $\boldsymbol{\Lambda}(\mathbf{X}, \beta, \mathbf{v}_w) = \boldsymbol{\Lambda}_a(\mathbf{X}, \beta, \mathbf{v}_w) + \boldsymbol{\Lambda}_e(\mathbf{X})$, with

$$\boldsymbol{\Lambda}_a(\mathbf{X}, \beta, \mathbf{v}_w) = \left[[\mathbf{F}_A^T]_p \quad [\mathbf{T}_A^T]_p \quad \tau_a \right]^T \quad (24)$$

where $\boldsymbol{\Lambda}_a$ is a vector related to pitch angle β . Then we have

$$\dot{\mathbf{X}} = f_0(\mathbf{X}) + g_0(\mathbf{X}, \beta, \mathbf{v}_w) + \mathbf{d}(t) \quad (25)$$

with

$$\begin{aligned} f_0(\mathbf{X}) &= \bar{\mathbf{M}}^{-1}(\mathbf{s}(\mathbf{X}) + \boldsymbol{\Lambda}_e(\mathbf{X})) \\ g_0(\mathbf{X}, \beta, \mathbf{v}_w) &= \bar{\mathbf{M}}^{-1}\boldsymbol{\Lambda}_a(\mathbf{X}, \beta, \mathbf{v}_w) \end{aligned} \quad (26)$$

and $\mathbf{d}(t)$ includes the uncertain parameters of model and external disturbances, which is assumed to satisfy: $\|d(t)\| \leq d_{m0}$, $\|\dot{d}(t)\| \leq d_{m1}$, and $\|\ddot{d}(t)\| \leq d_{m2}$, where d_{m0}, d_{m1}, d_{m2} are unknown positive constants.

B. Problem formulation

In SSFWTs, maintaining generator power at its rated value corresponds to regulating the rotor speed Ω_r to its rated value Ω_0 , denoted as $\Omega_r \rightarrow \Omega_0$. Similarly, minimizing platform pitch motion involves reducing the platform pitch rate, represented as $\dot{\theta}_y \rightarrow 0$. Unlike onshore wind turbines, SSFWTs may experience negative damping phenomena [34] when the relative wind speed permits the rotor to rotate at its rated value Ω_{r0} . To address this concern, an efficient resolution, inspired by the findings in [35], involves redefining the target rotor speed as a function of the platform pitch velocity $\dot{\theta}_y$, i.e.,

$$\Omega_r^* = \Omega_{r0} - k\dot{\theta}_y, \quad k > 0 \quad (27)$$

Then a trade-off between the aforementioned control objectives can be attained. Besides, it should be noted that while the control objective in our study only focuses on two DOFs of FWT, i.e., the rotor speed and platform pitch motion, it is essential to acknowledge the FWT is a multi-body coupled system and there exists inherent interplay among various DOFs, as presented in (22). Consequently, in order to accurately capture the dynamic response of the system, we have opted to establish a comprehensive 7-DOFs mathematical model of the FWT.

C. Pitch controller design

Define $\xi(t) = \Delta\Omega_r + k\Delta\dot{\theta}_y$, with $\Delta\Omega_r = \Omega_r - \Omega_{r0}$, $\Delta\dot{\theta}_y = \dot{\theta}_y - 0$. Then from (3), one has

$$\xi(t) = \mathbf{m}^T \mathbf{X} - \Omega_{r0} \quad (28)$$

with $\mathbf{m} = [\mathbf{0}_{1 \times 9} \quad 0 \quad kc_{\theta_x} \quad -ks_{\theta_x} \quad 1]^T$. Further, taking the time derivative of $\xi(t)$ gives

$$\begin{aligned} \dot{\xi}(t) &= \dot{\mathbf{m}}^T \mathbf{X} + \mathbf{m}^T \dot{\mathbf{X}} \\ &= \dot{\mathbf{m}}^T \mathbf{X} + \mathbf{m}^T (f_0(\mathbf{X}) + g_0(\mathbf{X}, \beta, \mathbf{v}_w) + \mathbf{d}(t)) \end{aligned} \quad (29)$$

Let

$$\bar{\xi} = \dot{\xi} + c\xi, \quad c > 0 \quad (30)$$

Taking the second derivative of $\xi(t)$ obtains

$$\begin{aligned} \ddot{\xi} = & \ddot{\mathbf{m}}^T \mathbf{X} + \dot{\mathbf{m}}^T \dot{\mathbf{X}} + \dot{\mathbf{m}}^T (f_0(\mathbf{X}) + g_0(\mathbf{X}, \beta, \mathbf{v}_w) \\ & + \mathbf{d}(t)) + \mathbf{m}^T \left(\frac{\partial f_0}{\partial \mathbf{X}} + \frac{\partial g_0}{\partial \mathbf{X}} \right) \dot{\mathbf{X}} + \mathbf{m}^T \frac{\partial g_0}{\partial \beta} \dot{\beta} \\ & + \mathbf{m}^T \frac{\partial g_0}{\partial v_w} \dot{v}_w + \mathbf{m}^T \dot{\mathbf{d}}(t) \end{aligned} \quad (31)$$

Moreover, differentiating (30) obtains

$$\begin{aligned} \dot{\xi} = & \ddot{\xi} + c\dot{\xi} \\ = & f_1(\mathbf{X}, \beta, \mathbf{v}_w) + g_1(\mathbf{X}, \beta, \mathbf{v}_w) \dot{\beta} + d_1(t) \end{aligned} \quad (32)$$

with $g_1(\mathbf{X}, \beta, \mathbf{v}_w) = \mathbf{m}^T \frac{\partial g_0}{\partial \beta}$, and

$$\begin{aligned} f_1(\mathbf{X}, \beta, \mathbf{v}_w) = & \ddot{\mathbf{m}}^T \mathbf{X} + 2\dot{\mathbf{m}}^T (f_0(\mathbf{X}) + g_0(\mathbf{X}, \beta, \mathbf{v}_w)) \\ & + \mathbf{m}^T \left(\frac{\partial f_0}{\partial \mathbf{X}} + \frac{\partial g_0}{\partial \mathbf{X}} \right) (f_0(\mathbf{X}) + g_0(\mathbf{X}, \beta, \mathbf{v}_w)) \\ d_1(t) = & 2\dot{\mathbf{m}}^T \mathbf{d}(t) + \mathbf{m}^T \left(\frac{\partial f_0}{\partial \mathbf{X}} + \frac{\partial g_0}{\partial \mathbf{X}} \right) \cdot \mathbf{d}(t) \\ & + \mathbf{m}^T \frac{\partial g_0}{\partial v_w} \dot{v}_w + \mathbf{m}^T \dot{\mathbf{d}}(t) \end{aligned}$$

Combining (24) and (26), it can be derived that

$$\begin{aligned} g_1(\mathbf{X}, \beta, \mathbf{v}_w) = & \mathbf{m}^T \bar{\mathbf{M}}^{-1} \frac{\partial}{\partial \beta} \Lambda_a(\mathbf{X}, \beta, \mathbf{v}_w) \\ = & b_1 \frac{\partial \tau_a}{\partial \beta} + b_2 k c \theta_x \frac{\partial F_a}{\partial \beta} \end{aligned} \quad (33)$$

where b_1 and b_2 are both positive constant, whose specific mathematical expressions are given in the Appendix B. Since $\frac{\partial \tau_a}{\partial \beta} < 0$, $\frac{\partial F_a}{\partial \beta} < 0$. Thus, one has

$$g(\mathbf{X}, \beta, \mathbf{v}_w) < 0$$

Define $T(\mathbf{X}, \beta, \mathbf{v}_w) = -1/g(\mathbf{X}, \beta, \mathbf{v}_w)$. In fact, $T(\mathbf{X}, \beta, \mathbf{v}_w)$ is a positive scalar with $1/g_{\min}$ being its largest singular value, where g_{\min} is the minimum value of function $-g(\mathbf{X}, \beta, \mathbf{v}_w)$. By utilizing (32), one has

$$\begin{aligned} T(\mathbf{X}, \beta, \mathbf{v}_w) \dot{\xi} = & -\frac{1}{2} \dot{T}(\mathbf{X}, \beta, \mathbf{v}_w) \bar{\xi} - \xi - \dot{\beta} \\ & + F(\mathbf{X}, \beta, \mathbf{v}_w) + D(t) \end{aligned} \quad (34)$$

with

$$\begin{aligned} F(\mathbf{X}, \beta, \mathbf{v}_w) = & -\frac{f(\mathbf{X}, \beta, \mathbf{v}_w)}{g(\mathbf{X}, \beta, \mathbf{v}_w)} + \frac{1}{2} \dot{T}(\mathbf{X}, \beta, \mathbf{v}_w) \bar{\xi} + \xi \\ D(t) = & T(\mathbf{X}, \beta, \mathbf{v}_w) d_1(t) \end{aligned} \quad (35)$$

Remark 3: Utilizing the mean value theorem [36], we deduce the boundedness of the functions $D(t)$ and $\dot{D}(t)$, expressed as $|D(t)| \leq D_{m0}$ and $|\dot{D}(t)| \leq D_{m1}$, respectively. Here, D_{m0} and D_{m1} denote unknown positive constants.

Notably, the uncertain dynamics is divided into two parts in (34), i.e., $F(\mathbf{X}, \beta, \mathbf{v}_w)$ and $D(t)$, which means that the disturbance signal $\mathbf{d}(t)$ is absent from the function $F(\mathbf{X}, \beta, \mathbf{v}_w)$. Thus, an online approximator (OLA) can be utilized to approximate and compensate $F(\mathbf{X}, \beta, \mathbf{v}_w)$. Specifically, there exists an ideal neural network (NN) approximation such that

$$F(\mathbf{X}, \beta, \mathbf{v}_w) = W^{*T} \phi(Z) + \epsilon(Z) \quad (36)$$

where $Z = [\mathbf{X}^T, \beta, \mathbf{v}_w]^T$. $W^* \in \mathbb{R}^{N \times 1}$ is the ideal weight matrix satisfying $\|W^*\| \leq w_m$, and N is the number of hidden layer nodes. $\phi(\cdot) : \mathbb{R}^N \rightarrow \mathbb{R}^N$ is the activation function satisfying $\|\phi\| \leq \phi_{m0}$, $\|\dot{\phi}\| \leq \phi_{m1}$; $\epsilon(Z)$ indicate the bounded NN reconstruction error satisfying $\|\epsilon\| \leq \epsilon_{m0}$, $\|\dot{\epsilon}\| \leq \epsilon_{m1}$. Note that the ideal weight matrix W^* is usually not known and must be estimated online for controller design purposes. Let \hat{W} represent the estimate of W^* . Then, a robust adaptive pitch controller is designed as

$$\dot{\beta} = (k_c + 1) \bar{\xi} + \hat{W}^T \phi(Z) + \gamma(t) \text{sgn}(\xi) \quad (37)$$

which leads to

$$\begin{aligned} \beta = & (k_c + 1) \xi(t) - (k_c + 1) \xi(0) + \int_0^t [\hat{W}^T \phi(Z(\varsigma)) \\ & + (k_c + 1) c \xi(\varsigma) + \gamma(\varsigma) \text{sgn}(\xi(\varsigma))] d\varsigma \end{aligned} \quad (38)$$

where $k_c > 0$ represents a constant gain, $\gamma(t)$ (with its expression to be specified later) serves as an adaptive term, and $\text{sgn}(\cdot)$ denotes the signum function. Moreover, the learning algorithm of \hat{W} is given as

$$\dot{\hat{W}} = l_w (c \phi(Z) \xi - k_w |\xi| \hat{W}) \quad (39)$$

Based on [37], it can be deduced that $\|\hat{W}\| \leq c \phi_{m0} / k_w$.

Next, the adaptive term γ in (37) can be designed as

$$\begin{aligned} \gamma = & \int_0^t \bar{\xi}^T(\varsigma) \text{sgn}(\xi(\varsigma)) d\varsigma \\ = & \int_{\xi(0)}^{\xi(t)} \text{sgn}(\xi) d\xi + c \int_0^t |\xi(\varsigma)| d\varsigma \end{aligned} \quad (40)$$

Without loss of generality, we assume that ξ changes its sign at a finite number of moments t_i , $i = 0, \dots, m-1$, where $m > 1$. That is, $\xi(t_i) = 0$, and for all $p_1, p_2 \in [t_i, t_{i+1}]$, we have $\text{sgn}(\xi(p_1)) = \text{sgn}(\xi(p_2))$. Let $t_0 = 0$ and $t_m = t$. Then γ can be reconstructed as

$$\begin{aligned} \gamma = & \int_{\xi(0)}^{\xi(t)} \text{sgn}(\xi) d\xi + c \int_0^t |\xi(\varsigma)| d\varsigma \\ = & \sum_{i=0}^{m-1} \int_{\xi(t_i)}^{\xi(t_{i+1})} \text{sgn}(\xi) d\xi + c \int_0^t |\xi(\varsigma)| d\varsigma \\ = & \sum_{i=0}^{m-1} (|\xi(t_i)| - |\xi(t_{i+1})|) + c \int_0^t |\xi(\varsigma)| d\varsigma \\ = & |\xi(t)| - |\xi(0)| + c \int_0^t |\xi(\varsigma)| d\varsigma \end{aligned} \quad (41)$$

Further, taking the time derivative of γ gives

$$\dot{\gamma} = \bar{\xi}^T \text{sgn}(\xi) \quad (42)$$

Finally, the overall structure of the presented adaptive pitch controller is shown Fig. 3.

D. Stability analysis

Stability and performance analyses based on the standard Lyapunov method are conducted in the subsequent description.

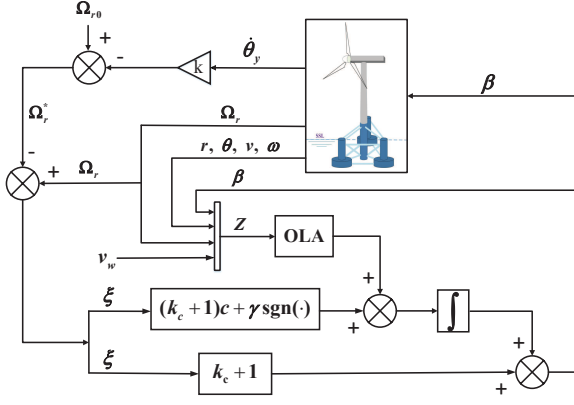


Fig. 3: Overall structure of the proposed controller.

First, substituting (36) and (37) into (35) leads to

$$T(\mathbf{X}, \beta, \mathbf{v}_w) \dot{\xi} = -\frac{1}{2} \dot{T} \bar{\xi} - \xi - (k_c + 1) \bar{\xi} - \gamma(t) \text{sgn}(\xi) + \tilde{W}^T \phi(Z) + \bar{D}(t) \quad (43)$$

where $\tilde{W} = W - \hat{W}$, $\bar{D}(t) = D(t) + \epsilon(Z)$. It is clear that $\|\bar{D}(t)\| \leq D_{m0} + \epsilon_{m0} \equiv \bar{D}_{m0}$ and $\|\dot{\bar{D}}(t)\| \leq D_{m1} + \epsilon_{m1} \equiv \bar{D}_{m1}$, and recalling (23) and (37), we have

$$\begin{aligned} \|\tilde{W}^T \phi(Z)\| &\leq W_{m0}, \\ \|\dot{\tilde{W}}^T \phi(Z) + \tilde{W}^T \dot{\phi}(Z)\| &\leq W_{m1} \end{aligned} \quad (44)$$

where W_{m0} and W_{m1} are unknown positive constants. Also, to support the stability analysis, the following lemma is given.

Lemma 1: [38] Define

$$\begin{aligned} \gamma_d &\equiv \bar{D}_{m0} + \max\left\{W_{m0}, \frac{(\bar{D}_{m1} + W_{m1} + k_w \|w_m\|^2/4)}{c}\right\}, \\ H &\equiv \xi^T (\bar{D} - \gamma_d \text{sgn}(\xi)) + k_w |\xi| \text{tr}(\tilde{W}^T \tilde{W}) - \xi^T \bar{N} \end{aligned}$$

with $\bar{N} = \tilde{W}^T \phi(Z)$. Then it can be concluded

$$\int_0^t H(\varsigma) d\varsigma \leq H_0 \quad (45)$$

with $H_0 \equiv \gamma_d |\xi(0)| - \xi^T(0) (\bar{D}(0) + \bar{N}(0))$.

In fact, the adaptive tuning law in (42) is designed to facilitate the gradual convergence of the parameter γ towards an unknown desired value γ_d . The approximation error is defined as $\tilde{\gamma} = \gamma_d - \gamma$. Subsequently, the stability of blade pitch controller is presented in the following theorem.

Theorem 1: Given the nonlinear model of SSFWT in (25). The desired rotor speed is described in (27). Then the pitch angle controller in (38) with the adaptive laws (39) and (40) can achieve the convergence of the regulation error.

Proof: See the Appendix C. ■

IV. MODEL VALIDATION AND CONTROL RESULTS

This section aims to assess the efficacy of the presented nonlinear modeling approach and the blade pitch controller for SSFWTs. The simulation utilizes parameters outlined in [39], [40] for the proposed model.

A. Model validation

First, an open-loop response test is implemented for the validation of the proposed SSFWT model under wind and wave joint loads. In particular, the turbulent wind data features a mean hub-height wind speed of 18 m/s and a turbulence intensity of 10%, with corresponding results depicted in the top of Fig. 4. For regular harmonic wave conditions, characterized by a peak period, $T_p = 10$ s, and a significant wave height of $H_s = 3$ m, the wave height time history is presented in the bottom of Fig. 4. In addition, the simulation commences with initial displacement and angular conditions set at 5 m and 9° , respectively. The total simulation duration spans 1000s, during which the blade pitch angle β remains fixed at zero. Moreover, the system responses generated by the presented nonlinear model are systematically compared with those derived from the widely used software FAST with all DOFs activated in the time domain.

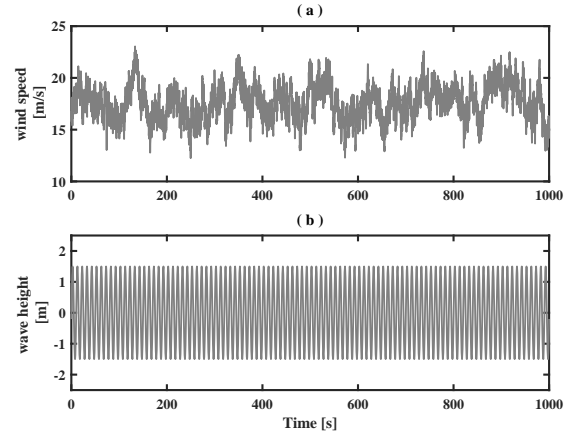


Fig. 4: Profiles of wind and wave height.

Fig. 5 presents a comparative analysis of the platform motion responses and rotor spin speed response for SSFWT. To further substantiate the efficacy of the presented model, average (AV) values and root mean square (RMS) values of the responses are quantitatively assessed and presented in Table I. The findings conclusively demonstrate the proficiency of the proposed SSFWT model in accurately predicting the primary motions of the complete 44-state FAST model, while considering the interplay of coupled 3-D motion dynamics. Notably, the responses in surge, sway, roll, and pitch DOFs exhibit a qualitative resemblance between the FAST and the presented model. The identified disparities in these DOFs amount to 4.6%, 2.2%, 2.9%, and 1.5%, respectively, substantiating the precision of the proposed model in capturing the fundamental dynamic behaviors of the SSFWT system.

B. Pitch controller validation

As depicted in Fig. 5, the turbulent wind conditions in this specific load scenario subject the rotor to a critical state, concurrently leading to heightened fluctuations in the rotor speed curve. Consequently, a pitch controller has been designed in (38) for the regulation of rotor angular speed Ω_r in

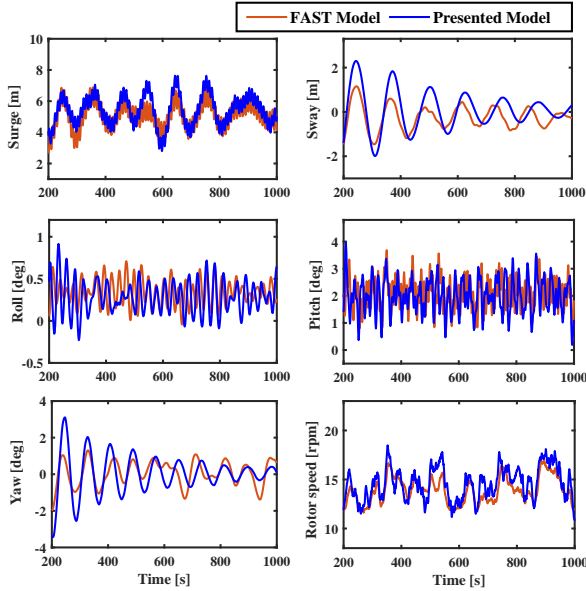


Fig. 5: The system responses under wind-wave joint loads.

TABLE I: Statistical characteristics of the system responses.

	FAST Model	Presented Model	Discrepancy
$AV(r_x)$ [m]	5.11	5.42	5.63%
$RMS(r_x)$ [m]	5.18	5.50	5.94%
$AV(\theta_y)$ [deg]	2.10	1.99	5.31%
$RMS(\theta_y)$ [deg]	2.18	2.09	3.96%
$AV(\Omega_r)$ [rpm]	13.88	14.57	4.77%
$RMS(\Omega_r)$ [rpm]	13.94	14.66	4.93%

Region III. The wind-wave conditions in this test is as same as in Fig. 4. The controller parameters are specified as $k = 4.5$, $c = 2$, $k_c = 10$, $N = 50$, $l_w = 1e - 3$, and $k_w = 1e - 3$. Additionally, the efficacy of the proposed control approach is evaluated against the baseline gain-scheduled proportional-integral (GSPI) controller [39] and the adaptive super-twisting (ASTW) controller introduced in [24].

Fig. 6 displays the comparison results for rotor speed, platform pitch rate, and blade pitch angle. To comprehensively assess the regulatory and loads mitigation performance, this study employs normalized RMS values for rotor speed error and platform motion rates along roll, pitch, and yaw axes, as depicted in Fig. 7. Simultaneously, Table II presents the damage equivalent loads (DEL) at the tower base (TB), blade root (BR), fair-lead force (FF), and anchor force (AF) for the three mooring lines. The outcomes in Figs. 6–7 reveal that our control scheme effectively maintains rotor speed around its rated value with minimal fluctuations. Specifically, compared with GSPI and ASTW methods, the RMS values for rotor speed error of the proposed method is decreased by 49.00% and 44.56%, respectively. Further, the platform roll and pitch rates are reduced by 11.96% and 3.45%, respectively, compared to the ASTW method. From Table II, it is noteworthy that the ASTW and RISE controllers exhibit higher DEL of BR

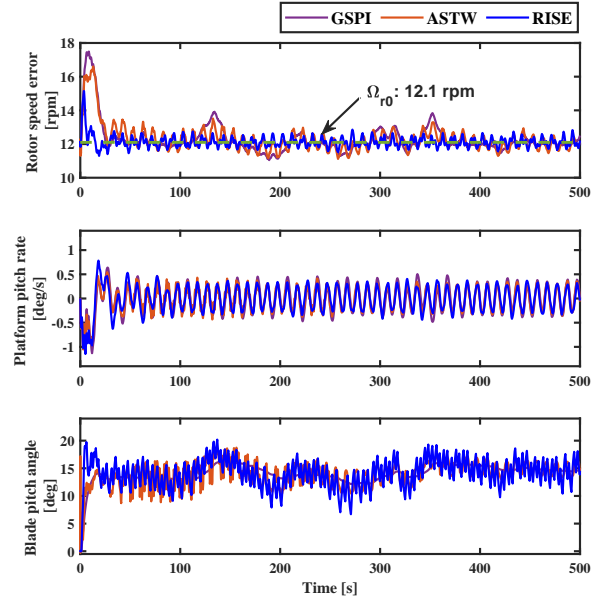


Fig. 6: Dynamic responses of rotor speed, platform pitch rate and blade pitch angle.

than the GSPI method, indicating a more pronounced demand on the blade pitch actuator. While the suggested approach does not enhance DEL of BR moments in comparison to the GSPI method, it notably enhances the DELs for tower base moments and two mooring lines. This improvement is also crucial for ensuring the stability and viability of the SSFWT system.

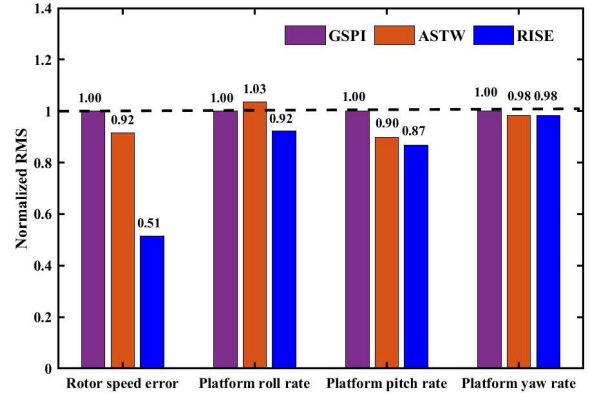


Fig. 7: The normalized RMS values.

V. CONCLUSION

In this paper, a 7-DOF reduced-order model for SSFWT has been developed, incorporating the coupled dynamics of its external key components. Different from the exist modeling methods, both the rotor dynamics and finite rotations of floating platform are considered in our method. Further, based on the established model, a novel robust nonlinear controller is proposed specifically designed to achieve power production regulation while mitigating platform pitch motion for SSFWT

TABLE II: Normalized DEL values.

	GSPI	ASTW	RISE
TB	1.00	1.04	0.95
BR	1.00	1.00	1.00
FF₁	1.00	1.03	0.94
AF₁	1.00	1.05	0.95
FF₂	1.00	1.05	0.99
AF₂	1.00	1.08	0.98
FF₃	1.00	1.08	1.03
AF₃	1.00	1.09	1.04

under wind and wave disturbances. Moreover, an OLA is utilized to capture the unknown dynamics resulting from unmeasurable external environmental inputs and to address model uncertainties arising from time-varying parameters. Finally, the accuracy of the proposed model against FAST model is validated, while the superiority of the proposed pitch controller are clearly demonstrated through comprehensive comparative studies with traditional pitch controllers.

APPENDIX

A. Added mass matrix.

$$\mathbf{M}_a = \mathbf{M}_{a1} + \mathbf{M}_{a2} \quad (46)$$

with

$$\mathbf{M}_{a1} = \sum_{i=1}^7 \begin{bmatrix} M_{i1} & -M_{i2} \\ \bar{M}_{i3} & \bar{M}_{i4} \end{bmatrix}, \quad \mathbf{M}_{a2} = \sum_{j=5}^7 \begin{bmatrix} N_{j1} & N_{j2} \\ N_{j3} & N_{j4} \end{bmatrix}$$

where $M_{i1} = C_{Ai}L_iT_n$, $M_{i2} = C_{Ai}T_n\tilde{\mathbf{r}}_{bi}L_i + M_{i3}$,

$$M_{i3} = C_{Ai} \int_{z_b}^{z_t} \begin{bmatrix} 0 & -z & 0 \\ z & 0 & 0 \\ 0 & 0 & 0 \end{bmatrix} dz,$$

$$\bar{M}_{i3} = \tilde{\mathbf{r}}_{bi}M_{i1} + M_{i3},$$

$$\bar{M}_{i4} = -\tilde{\mathbf{r}}_{bi}M_{i2} - M_{i4} + M_{i5}, \quad M_{i4} = M_{i3}\tilde{\mathbf{r}}_{bi},$$

$$M_{i5} = C_{Ai} \int_{z_b}^{z_t} \begin{bmatrix} z^2 & 0 & 0 \\ 0 & z^2 & 0 \\ 0 & 0 & 0 \end{bmatrix} dz$$

and

$$N_{j1} = C_{A_{2j}}T_h, \quad N_{j2} = -C_{A_{2j}}T_h\tilde{\mathbf{r}}_{c_j}, \\ N_{j3} = \tilde{\mathbf{r}}_{c_j}N_{j1}, \quad N_{j4} = \tilde{\mathbf{r}}_{c_j}N_{j2}$$

with

$$T_n = \begin{bmatrix} 1 & 0 & 0 \\ 0 & 1 & 0 \\ 0 & 0 & 0 \end{bmatrix}, \quad T_h = \begin{bmatrix} 0 & 0 & 0 \\ 0 & 0 & 0 \\ 0 & 0 & 1 \end{bmatrix}$$

In order to simplify the expression of added mass, we assume that it does not get recomputed as the lengths of the submerged cylinders change, i.e., L_i equals to its original value. Then we

have

$$\mathbf{M}_a = \begin{bmatrix} b_{11} & 0 & 0 & 0 & b_{15} & 0 \\ & b_{11} & 0 & -b_{15} & 0 & 0 \\ & & b_{33} & 0 & 0 & 0 \\ & & & b_{44} & 0 & 0 \\ * & & & & b_{55} & 0 \\ & & & & & b_{66} \end{bmatrix}$$

where $b_{11} = \sum_{i=1}^7 C_{Ai}L_i$, $b_{33} = \sum_{j=5}^7 C_{A_{2j}}$, $b_{15} = \sum_{i=1}^7 C_{Ai}L_i^2(1 + 2r_{bi3})/2$, $b_{66} = C_{Ai}L_i r_{bi1}^2 + C_{Ai}L_i r_{bi2}^2$, $b_{44} = b_{55} = \sum_{i=1}^7 \sum_{j=5}^7 (C_{Ai}L_i^3/3 + C_{Ai}L_i^2 r_{bi3} + C_{Ai}L_i r_{bi3}^2 + C_{A_{2j}} r_{cj1}^2)$.

B. System matrices in (22).

$$\bar{\mathbf{M}} = \begin{bmatrix} \mathbf{I}_{6 \times 6} & \mathbf{0}_{6 \times 7} \\ \mathbf{0}_{7 \times 6} & \bar{\mathbf{M}}_s \end{bmatrix}$$

$$\text{where } \bar{\mathbf{M}}_s = \begin{bmatrix} \mathbf{M}_{s1} & \mathbf{M}_{s2} \\ \mathbf{M}_{s3} & \mathbf{M}_{s4} \end{bmatrix} + \begin{bmatrix} \mathbf{M}_a & \mathbf{0}_{6 \times 1} \\ \mathbf{0}_{1 \times 6} & 0 \end{bmatrix},$$

$$\mathbf{M}_{s1} = \begin{bmatrix} a_1 & 0 & 0 & 0 & a_2 & 0 \\ & a_1 & 0 & -a_2 & 0 & a_3 \\ & & a_1 & 0 & -a_3 & 0 \\ & & & a_4 & 0 & a_6 \\ * & & & & a_5 & 0 \\ & & & & & a_7 \end{bmatrix}$$

$$\mathbf{M}_{s2}^T = \mathbf{M}_{s3} = [0 \ 0 \ 0 \ I_{rx} \ 0 \ 0], \quad \mathbf{M}_{s4} = I_{rx}$$

with

$$a_1 = m_p + m_t + m_{nc} + m_r, \\ a_2 = H_r(m_r + m_{nc}) + m_t H_t, \\ a_3 = h_{nc} m_{nc} - h_r m_r, \\ a_4 = I_{px} + I_{tx} + I_{ncx} + I_{rx} + H_r^2(m_r + m_{nc}) + H_t^2 m_t, \\ a_5 = I_{py} + I_{ty} + I_{ncy} + I_{ry} + m_r(H_r^2 + h_r^2) \\ + m_{nc}(H_r^2 + h_{nc}^2) + H_t^2 m_t, \\ a_6 = H_r h_r m_r - H_r h_{nc} m_{nc}, \\ a_7 = I_{pz} + I_{tz} + I_{ncz} + I_{rz} + m_r h_r^2 + m_{nc} h_{nc}^2$$

and

$$\mathbf{s}(\mathbf{r}_p, \boldsymbol{\theta}_p, \mathbf{v}_p, \boldsymbol{\omega}_p, \Omega_r)$$

$$= - \begin{bmatrix} \mathbf{0}_{6 \times 6} & \mathbf{0}_{6 \times 7} \\ \mathbf{0}_{7 \times 6} & \mathbf{C}_s \end{bmatrix} \begin{bmatrix} [\mathbf{r}_p]_I \\ [\boldsymbol{\theta}_p]_I \\ [\mathbf{v}_p]_p \\ [\boldsymbol{\omega}_p]_p \\ \Omega_r \end{bmatrix} + g \begin{bmatrix} a_1 s_{\theta_y} \\ -a_1 c_{\theta_y} s_{\theta_x} \\ -a_1 c_{\theta_x} c_{\theta_y} \\ c_{\theta_y} s_{\theta_x} a_2 \\ s_{\theta_y} a_2 + c_{\phi} c_{\theta_y} m_d \\ -s_{\theta_x} c_{\theta_y} m_d \end{bmatrix}$$

where $m_d = h_{nc} m_{nc} + h_r m_r$, and $\mathbf{C}_s = \begin{bmatrix} \mathbf{C}_{s1} & \mathbf{C}_{s2} \\ \mathbf{C}_{s3} & \mathbf{C}_{s4} \end{bmatrix}$, with

$$\mathbf{C}_{s1} = \tilde{\mathbf{S}} \mathbf{M}_{s1} = \begin{bmatrix} [\tilde{\boldsymbol{\omega}}_p]_p & \mathbf{0}_{3 \times 3} \\ [\tilde{\mathbf{v}}_p]_p & [\tilde{\boldsymbol{\omega}}_p]_p \end{bmatrix} \mathbf{M}_{s1}$$

$$\mathbf{C}_{s2} = [0 \ 0 \ 0 \ 0 \ I_{rx} \omega_z \ -I_{rx} \omega_y]^T$$

$$\mathbf{C}_{s3} = [0 \ 0 \ 0 \ 0 \ 0 \ 0], \quad \mathbf{C}_{s4} = 0$$

$$b_1 = \frac{1}{I_{rx}}, \quad b_2 = \frac{h_1(h_2 - H_r h_3)}{(h_1 h_2^2 + h_3 h_4^2 - h_5 h_3 h_1)}$$

with $h_1 = a_1 + b_{33}$, $h_2 = a_2 + b_{15}$, $h_3 = a_1 + b_{11}$, $h_4 = a_3$, $h_5 = a_5 + b_{55}$. Since $H_r > H_t$, it can be easily deduced that $h_2 - H_r h_3 < 0$. Also, by some simple calculations, it can be obtained that $h_1 h_2^2 + h_3 h_4^2 - h_5 h_3 h_1 < 0$. Thus, we have $b_2 > 0$.

C. Proof of Theorem 1.

Consider the following Lyapunov function candidate:

$$V_L = \frac{1}{2} \xi^T \xi + \frac{1}{2} \bar{\xi}^T T(Y) \bar{\xi} + Q + P + \frac{1}{2} \tilde{\gamma}^2 \quad (47)$$

with $Y = [\mathbf{X}^T, \beta, \mathbf{v}_w]^T$, and

$$P = H_0 - \int_0^t H(\varsigma) d\varsigma, \quad Q = \frac{1}{2l_w} \text{tr}(\tilde{W}^T \tilde{W}) \quad (48)$$

Then, there exist two \mathcal{K} -class functions V_{k_1} , V_{k_2} , such that

$$V_{k_1}(M) \leq V_L \leq V_{k_2}(M) \quad (49)$$

with $M = [\xi^T \quad \bar{\xi}^T \quad \sqrt{Q} \quad \sqrt{P} \quad \tilde{\gamma}]^T$, and

$$V_{k_1} = \alpha_1 \|M\|^2, \quad \alpha_1 = \frac{1}{2} \min\{1, T(Y)\} > 0, \quad (50)$$

$$V_{k_2} = \alpha_2 \|M\|^2, \quad \alpha_2 = \max\{1, T(Y)\} > 0$$

Next, the time derivative of V_L is obtained as

$$\begin{aligned} \dot{V}_L &= \xi^T \dot{\xi} + \bar{\xi}^T T(Y) \dot{\bar{\xi}} + \frac{1}{2} \bar{\xi}^T \dot{T}(Y) \bar{\xi} + \frac{1}{l_w} \text{tr}(\tilde{W}^T \dot{\tilde{W}}) \\ &\quad - \bar{\xi}^T (\bar{D} - \gamma_d \text{sgn}(\xi)) - \frac{\|w_m\|^2}{4} \xi^T \text{sgn}(\xi) \\ &\quad + \dot{\xi}^T \bar{N} + \tilde{\gamma} \dot{\tilde{\gamma}} \\ &= \xi^T \dot{\xi} + \bar{\xi}^T \times [-\xi - \tilde{W}^T \phi(Z) - (k_c + 1) c\bar{\xi} \\ &\quad - \gamma \text{sgn}(\xi) + \bar{D}] + c\bar{\xi}^T \tilde{W}^T \phi(Z) \\ &\quad - k_w |\xi| \text{tr}(\tilde{W}^T \tilde{W}) - \bar{\xi}^T (\bar{D} - \gamma_d \text{sgn}(\xi)) \\ &\quad - \frac{\|w_m\|^2}{4} \xi^T \text{sgn}(\xi) + \dot{\xi}^T \bar{N} + \tilde{\gamma} \dot{\tilde{\gamma}} \text{sgn}(\xi) \\ &= \xi^T \dot{\xi} + \bar{\xi}^T (-\xi - (k_c + 1) c\bar{\xi}) - \bar{\xi}^T \tilde{W}^T \phi(Z) \\ &\quad + c\bar{\xi}^T \tilde{W}^T \phi(Z) + \dot{\xi}^T \bar{N} - k_w |\xi| \text{tr}(\tilde{W}^T \tilde{W}) \\ &\quad - k_w |\xi| \text{tr}(\tilde{W}^T \tilde{W}) - \frac{\|w_m\|^2}{4} \xi^T \text{sgn}(\xi) \\ &\quad - \gamma \bar{\xi}^T \text{sgn}(\xi) + \gamma_d \bar{\xi}^T \text{sgn}(\xi) + \tilde{\gamma} \dot{\tilde{\gamma}} \text{sgn}(\xi) \\ &= \xi^T \dot{\xi} + \bar{\xi}^T (-\xi - (k_c + 1) c\bar{\xi}) - k_w |\xi| \text{tr}(\tilde{W}^T \tilde{W}) \\ &\quad - k_w |\xi| \text{tr}(\tilde{W}^T \tilde{W}) - \frac{\|w_m\|^2}{4} |\xi| \end{aligned}$$

Further, it derives

$$\begin{aligned} V_L &\leq \xi^T \dot{\xi} + \bar{\xi}^T (-\xi - (k_c + 1) c\bar{\xi}) - k_w |\xi| (\|\tilde{W}\| \\ &\quad - \|W\|/2)^2 + \frac{k_w |\xi| \|W\|^2}{4} - \frac{\|w_m\|^2}{4} |\xi| \\ &\leq \xi^T \dot{\xi} + \bar{\xi}^T (-\xi - (k_c + 1) c\bar{\xi}) - k_w |\xi| (\|\tilde{W}\| \\ &\quad - \|W\|/2)^2 \\ &\leq -c\xi^T \xi - (k_c + 1) c\bar{\xi}^T \bar{\xi} \end{aligned}$$

which leads to

$$\dot{V}_L \leq -L(M) \quad (51)$$

with $L(M) = c \|\begin{bmatrix} \xi^T & \bar{\xi}^T \end{bmatrix}\|^2$, which is a continuously positive semi-definite function defined over an arbitrary compact set $\Gamma_M \subset \mathbb{R}^5$. Based on (49) and (50), it can be inferred that V_L is bounded over Γ_M . Therefore, ξ , $\bar{\xi}$, \tilde{W} , and $\tilde{\gamma}$ are all bounded. By recalling the definition of ξ in (28), it is evident that both $\Delta\Omega_r$ and $\Delta\dot{\theta}_y$ are bounded. In addition, the boundedness of $\bar{\xi}$ implies that $\dot{\xi}$ is also bounded. Note that the unknown disturbance $d(t)$ and its time derivatives are generally assumed to be bounded. Then from (29), it derives that the control input β is bounded.

Utilizing conventional linear analysis techniques, it can be inferred that the variables in equations (32), (34), (37), and (40) exhibit bounded behavior. Consequently, all signals within the closed-loop system are ensured to remain within bounds. Hence, it can be deduced that $L(M)$ is uniformly continuous. Moreover, Barbalat's lemma [41] can be applied to deduce that

$$|\xi(t)|^2 \rightarrow 0 \quad \text{and} \quad |\bar{\xi}(t)|^2 \rightarrow 0 \quad \text{as} \quad t \rightarrow \infty. \quad (52)$$

This can be further obtained that $|\xi(t)| \rightarrow 0$ as $t \rightarrow \infty$.

REFERENCES

- [1] W. D. Musial, P. C. Beiter, P. Spitsen, J. Nunemaker, and V. Gevorgian, "2018 offshore wind technologies market report," National Renewable Energy Lab.(NREL), Golden, CO (United States), Tech. Rep., 2019.
- [2] J. Xie, H. Dong, and X. Zhao, "Power regulation and load mitigation of floating wind turbines via reinforcement learning," *IEEE Transactions on Automation Science and Engineering*, 2023.
- [3] Z. Song, J. Liu, Y. Liu, Y. Hu, and F. Fang, "Fault-tolerant control of floating wind turbine with switched adaptive sliding mode controller," *IEEE Transactions on Automation Science and Engineering*, 2023.
- [4] Z. Ren, A. S. Verma, Y. Li, J. J. Teuwen, and Z. Jiang, "Offshore wind turbine operations and maintenance: A state-of-the-art review," *Renewable and Sustainable Energy Reviews*, vol. 144, p. 110886, 2021.
- [5] J. M. Jonkman, M. L. Buhl *et al.*, *FAST user's guide*. National renewable energy Laboratory Golden, CO, USA, 2005, vol. 365.
- [6] G. Stewart and M. Lackner, "Determining optimal tuned mass damper parameters for offshore wind turbines using a genetic algorithm," in *50th AIAA aerospace sciences meeting including the new horizons forum and aerospace exposition*, 2012, p. 376.
- [7] Stewart, Gordon and Lackner, Matthew, "Offshore wind turbine load reduction employing optimal passive tuned mass damping systems," *IEEE Transactions on Control Systems Technology*, vol. 21, no. 4, pp. 1090–1104, 2013.
- [8] G. Betti, M. Farina, G. A. Guagliardi, A. Marzorati, and R. Scatoloni, "Development of a control-oriented model of floating wind turbines," *IEEE Transactions on Control Systems Technology*, vol. 22, no. 1, pp. 69–82, 2013.
- [9] J. R. Homer and R. Nagamune, "Physics-based 3-D control-oriented modeling of floating wind turbines," *IEEE Transactions on Control Systems Technology*, vol. 26, no. 1, pp. 14–26, 2017.
- [10] Z. Song, Y. Hu, W. Cai, Y. Cheng, J. Liu, and F. Fang, "Control-oriented modeling and characteristic analysis of offshore semisubmersible wind turbine under wind-wave joint loads," *IEEE Transactions on Control Systems Technology*, 2023.
- [11] M. K. Al-Solihat, M. Nahon, and K. Behdinin, "Dynamic modeling and simulation of a spar floating offshore wind turbine with consideration of the rotor speed variations," *Journal of Dynamic Systems, Measurement, and Control*, vol. 141, no. 8, p. 081014, 2019.
- [12] J. Li and H. Geng, "Rotor speed control in above-rated wind speed region for floating offshore wind turbine," *IEEE Transactions on Sustainable Energy*, 2024.

- [13] T. J. Larsen and T. D. Hanson, "A method to avoid negative damped low frequent tower vibrations for a floating, pitch controlled wind turbine," in *Journal of Physics: Conference Series*, vol. 75, no. 1. IOP Publishing, 2007, p. 012073.
- [14] H. Lee and D.-J. Lee, "Effects of platform motions on aerodynamic performance and unsteady wake evolution of a floating offshore wind turbine," *Renewable Energy*, vol. 143, pp. 9–23, 2019.
- [15] J. Jonkman, "Influence of control on the pitch damping of a floating wind turbine," in *46th AIAA aerospace sciences meeting and exhibit*, 2008, p. 1306.
- [16] H. Namik and K. Stol, "Individual blade pitch control of floating offshore wind turbines," *Wind Energy: An International Journal for Progress and Applications in Wind Power Conversion Technology*, vol. 13, no. 1, pp. 74–85, 2010.
- [17] S. Sarkar, B. Fitzgerald, and B. Basu, "Individual blade pitch control of floating offshore wind turbines for load mitigation and power regulation," *IEEE Transactions on Control Systems Technology*, vol. 29, no. 1, pp. 305–315, 2020.
- [18] M. A. Evans, M. Cannon, and B. Kouvaritakis, "Robust MPC tower damping for variable speed wind turbines," *IEEE Transactions on Control Systems Technology*, vol. 23, no. 1, pp. 290–296, 2014.
- [19] E. Bossanyi, "Gh bladed theory manual," *GH & Partners Ltd*, vol. 2, pp. 56–58, 2003.
- [20] S. Sarkar, B. Fitzgerald, and B. Basu, "Development of a flexible multibody dynamics wind turbine model following kane's method," *Proc. Civil Eng. Res. Ireland*, pp. 883–888, 2018.
- [21] S. Tang, D. Tian, X. Wu, M. Huang, and Y. Deng, "Wind turbine load reduction based on 2DoF robust individual pitch control," *Renewable Energy*, vol. 183, pp. 28–40, 2022.
- [22] S. A. A. Shah, B. Gao, N. Ahmed, and C. Liu, "Advanced robust control techniques for the stabilization of translational oscillator with rotational actuator based barge-type OFWT," *Proceedings of the Institution of Mechanical Engineers, Part M: Journal of Engineering for the Maritime Environment*, vol. 235, no. 2, pp. 327–343, 2021.
- [23] C. Zhang, S. V. Gutierrez, F. Plestan, and J. De León-Morales, "Adaptive super-twisting control of floating wind turbines with collective blade pitch control," *IFAC-PapersOnLine*, vol. 52, no. 4, pp. 117–122, 2019.
- [24] C. Zhang and F. Plestan, "Individual/collective blade pitch control of floating wind turbine based on adaptive second order sliding mode," *Ocean Engineering*, vol. 228, p. 108897, 2021.
- [25] S. V. Gutierrez, C. Zhang, J. De León-Morales, and F. Plestan, "A simplified version of adaptive super twisting-application to the control of floating wind turbine," *Control Engineering Practice*, vol. 125, p. 105208, 2022.
- [26] J. L. Junkins and J. D. Turner, *Optimal spacecraft rotational maneuvers*. Elsevier, 2012.
- [27] O. Faltinsen, *Sea loads on ships and offshore structures*. Cambridge university press, 1993, vol. 1.
- [28] Y. Goda, *Random seas and design of maritime structures*. World Scientific Publishing Company, 2010, vol. 33.
- [29] H. Irvine, "Cable structures (series in structural mechanics)," 1981.
- [30] M. Isaacson and J. Baldwin, "Moored structures in waves and currents," *Canadian Journal of Civil Engineering*, vol. 23, no. 2, pp. 418–430, 1996.
- [31] L. Meirovitch and T. Stemple, "Hybrid equations of motion for flexible multibody systems using quasicordinates," *Journal of Guidance, Control, and Dynamics*, vol. 18, no. 4, pp. 678–688, 1995.
- [32] L. Meirovitch and I. Tuzcu, "Integrated approach to the dynamics and control of maneuvering flexible aircraft," 2003.
- [33] B. Xian, D. M. Dawson, M. S. de Queiroz, and J. Chen, "A continuous asymptotic tracking control strategy for uncertain nonlinear systems," *IEEE Transactions on Automatic Control*, vol. 49, no. 7, pp. 1206–1211, 2004.
- [34] T.-T. Tran and D.-H. Kim, "The platform pitching motion of floating offshore wind turbine: A preliminary unsteady aerodynamic analysis," *Journal of Wind Engineering and Industrial Aerodynamics*, vol. 142, pp. 65–81, 2015.
- [35] M. A. Lackner, "Controlling platform motions and reducing blade loads for floating wind turbines," *Wind Engineering*, vol. 33, no. 6, pp. 541–553, 2009.
- [36] S. C. Malik and S. Arora, *Mathematical analysis*. New Age International, 1992.
- [37] W. He, Y. Chen, and Z. Yin, "Adaptive neural network control of an uncertain robot with full-state constraints," *IEEE Transactions on Cybernetics*, vol. 46, no. 3, pp. 620–629, 2015.
- [38] Q. Yang, S. Jagannathan, and Y. Sun, "Robust integral of neural network and error sign control of MIMO nonlinear systems," *IEEE Transactions on Neural Networks and Learning Systems*, vol. 26, no. 12, pp. 3278–3286, 2015.
- [39] J. Jonkman, S. Butterfield, W. Musial, and G. Scott, "Definition of a 5-MW reference wind turbine for offshore system development," National Renewable Energy Lab.(NREL), Golden, CO (United States), Tech. Rep., 2009.
- [40] A. Robertson, J. Jonkman, M. Masciola, H. Song, A. Goupee, A. Coulling, and C. Luan, "Definition of the semisubmersible floating system for phase II of OC4," National Renewable Energy Lab.(NREL), Golden, CO (United States), Tech. Rep., 2014.
- [41] H. Khalil, *Nonlinear Systems (3rd Ed.)*. Upper Saddle River, NJ: Prentice-Hall, 01 2001.